ELSEVIER

J. Non-Newtonian Fluid Mech. 116 (2004) 371–393

Journal of Non-Newtonian Fluid Mechanics

www.elsevier.com/locate/jnnfm

Instability of viscoelastic plane Couette flow past a deformable wall

V. Shankar [a,*], Satish Kumar [b,*]

[a] *Department of Chemical Engineering, Indian Institute of Technology, Kanpur 208016, India*

[b] *Department of Chemical Engineering and Materials Science, University of Minnesota, Minneapolis, MN 55455, USA*

Received 15 July 2003; received in revised form 14 October 2003

Abstract

The stability of plane Couette flow of an upper-convected Maxwell (UCM) fluid of thickness R, viscosity η and relaxation time τ_R past a deformable wall (modeled here as a linear viscoelastic solid fixed to a rigid plate) of thickness HR, shear modulus G and viscosity η_w is determined using a temporal linear stability analysis in the creeping-flow regime where the inertia of the fluid and the wall is negligible. The effect of wall elasticity on the stable modes of Gorodtsov and Leonov [J. Appl. Math. Mech. 31 (1967) 310] for Couette flow of a UCM fluid past a rigid wall, and the effect of fluid elasticity on the unstable modes of Kumaran et al. [J. Phys. II (Fr.) 4 (1994) 893] for Couette flow of a Newtonian fluid past a deformable wall are analyzed. Results of our analysis show that there is only one unstable mode at finite values of the Weissenberg number, $W = \tau_R V/R$ (where V is the velocity of the top plate) and nondimensional wall elasticity, $\Gamma = V\eta/(GR)$. In the rigid wall limit, $\Gamma \ll 1$ and at finite W this mode becomes stable and reduces to the stable mode of Gorodtsov and Leonov. In the Newtonian fluid limit, $W \to 0$ and at finite Γ this mode reduces to the unstable mode of Kumaran et al. The variation of the critical velocity, Γ_c, required for this instability as a function of $\bar{W} = \tau_R G/\eta$ (a modified Weissenberg number) shows that the instability exists in a finite region in the $\Gamma_c - \bar{W}$ plane when $\Gamma_c > \Gamma_{c,Newt}$ and $\bar{W} < \bar{W}_{max}$, where $\Gamma_{c,Newt}$ is the value of the critical velocity for a Newtonian fluid. The variation of Γ_c with $\bar{W}$ for various values of H are shown to collapse onto a single master curve when plotted as $\Gamma_c H$ versus $\bar{W}/H$, for $H \gg 1$. The effect of wall viscosity is analyzed and is shown to have a stabilizing effect.

Keywords: Interfacial instability; Viscoelastic fluids; Deformable solids; Linear stability analysis; Creeping flow

1. Introduction

Fluid flow past soft, deformable solid surfaces is encountered in diverse settings: the flow of fluid through a tube with flexible walls occurs in biological systems, and some biotechnological applications involve flow past polymer matrices and membranes. The dynamics of fluid flow past deformable solids is qualita-

* Corresponding author.

E-mail addresses: vshankar@iitk.ac.in (V. Shankar), kumar@cems.umn.edu (S. Kumar).

0377-0257/$ – see front matter © 2003 Elsevier B.V. All rights reserved.
doi:10.1016/j.jnnfm.2003.10.003

Nomenclature

$c = c_r + ic_i$	complex wave-speed
G	shear modulus of the solid
H	nondimensional thickness of the wall
k	wavenumber
R	dimensional thickness of fluid
V	dimensional velocity of the top plate
$W = \tau_R V/R$	Weissenberg number
$\bar{W} = \tau_R G/\eta$	flow-independent Weissenberg number
$\bar{W}_{max}$	maximum $\bar{W}$ for instability to exist
Greek letters	
$\Gamma = V\eta/(GR)$	nondimensional velocity of top plate
$\Gamma_{c,Newt}$	minimum Γ for instability
η	viscosity of the fluid
η_w	viscosity of the wall
$\eta_r = \eta_w/\eta$	ratio of wall to fluid viscosity
τ_R	relaxation time in the UCM model

tively different from that of rigid surfaces because of the coupling between the fluid and solid dynamics, and the elasticity of the solid could affect the fluid flow. Because the shear modulus of a soft solid is typically low ($\sim$ 1 kPa to 1 MPa), waves can propagate along the solid-fluid interface. In particular, this coupling between the fluid and solid dynamics could render the flow unstable, or could even induce the transition from a laminar to a more complicated flow [1] by amplifying the growth of the interfacial waves. Motivated by the earlier experimental results of Krindel and Silberberg [1], there has been a renewed interest in the stability of fluid flow past deformable solid surfaces both on the theoretical [2,3], and experimental [4,5] fronts. These studies show that a novel feature in flow past deformable surfaces is that the flow could be unstable even in the limit of zero Reynolds number, i.e., the creeping flow limit. Subsequent theoretical studies [6–8] have shown that novel instabilities also exist in the high-Reynolds number regime, and these instabilities in flow past deformable surfaces are not a continuation of existing instabilities in rigid tubes and channels, but are qualitatively new instabilities which arise due to the existence of wall deformability.

All such prior studies were restricted to the stability of Newtonian fluids. However, there are many instances in which the fluid flowing could be non-Newtonian. For example, many biological fluids are non-Newtonian in nature and could exhibit shear-rate dependent properties and viscoelastic effects. Another context in which this type of flow could be relevant is in polymer processing, where one may have a two-layer flow in which each layer is being crosslinked to form a gel, possibly as part of a composite material. If one of the layers solidifies before the other, then instabilities of the type studied here could potentially occur. This could be detrimental to the quality of the final product, or it could serve as a way to create interfacial structures. A third example pertains to mixing: if deformable surfaces can be used to induce instabilities, the resulting flows may provide a novel mechanism for promoting mixing in viscoelastic liquids. An important question to be answered is whether non-Newtonian effects can induce additional instabilities apart from those existent in Newtonian fluid flow past deformable surfaces. In this

work, we take a first step in this direction by extending the earlier studies to rheologically complex fluids by focusing on the stability of an upper-convected Maxwell fluid flowing past a deformable wall. In the remainder of this Introduction, relevant previous studies in related areas are briefly summarized, and the motivation for the present work is placed in perspective.

Creeping flow of a Newtonian fluid through rigid channels and tubes is always stable because the governing Stokes equations are not explicitly dependent on time, meaning that fluid inertia is needed for destabilizing the flow. However, if we consider the creeping flow of a viscoelastic fluid, time dependence enters the problem through the constitutive relation even in the absence of fluid inertia, and in principle there is a possibility of an instability even in the low Reynolds number limit. For simplicity, we choose the upper-convected Maxwell model (hereafter abbreviated as UCM) as a constitutive relation for the viscoelastic fluid in this work. Although the Oldroyd-B model (which adds a solvent viscosity contribution to the UCM model) is more suitable for modeling polymer solutions such as Boger fluids, it is argued in Section 3.2 that the instability predicted in this work for the UCM model is expected to occur even for Oldroyd-B fluids. One of the basic problems is to understand the stability of plane Couette flow of a UCM fluid between two rigid plates, and this was first addressed by Gorodtsov and Leonov [9] (abbreviated as G–L henceforth). They showed analytically that the stability is governed by a quadratic characteristic equation for the wavespeed in the creeping-flow limit, and the two roots of this equation were always found to be stable. In addition to these two discrete eigenvalues for the wavespeed, there exists a continuous spectrum of eigenvalues which are always stable (also see [10,11]).

At finite Reynolds numbers (*Re*), numerical analysis by Renardy and Renardy [12] showed that the flow is stable. Renardy [13] further provided a rigorous proof for stability at $\mathrm{Re} = 0$, but arbitrary values of the Weissenberg number $W = \tau_R V/R$, where τ_R is the relaxation time in the UCM model, and R and V are respectively the fluid thickness and velocity of the top plate. Similarly, Sureshkumar and Beris [14] found using a numerical method that the viscoelastic plane Poiseuille flow of a UCM fluid is also stable at $\mathrm{Re} = 0$ for all W. All these studies were, however, restricted to rigid-walled channels. The above discussion gives rise to the question of whether wall deformability could destabilize the (discrete) stable modes found by G–L [9] for the case of plane Couette flow of a UCM fluid. The presence of wall deformability couples the dynamics of the UCM fluid with the dynamics of the wall medium, and this coupling could destabilize the flow. This discussion provides one of the main motivations for the present work: will the presence of deformability in the wall medium destabilize the plane Couette flow of a UCM fluid?

Kumaran et al. [2] (abbreviated KFP in what follows) studied the linear temporal stability of the plane Couette flow of Newtonian fluid of viscosity η past a deformable wall of finite thickness, which was modeled as an incompressible linear viscoelastic solid of shear modulus G fixed to a rigid substrate. Their analysis showed that the flow is unstable for $\mathrm{Re} = 0$, as the time dependence entered through the tangential velocity condition at the interface, which coupled the base flow to interfacial perturbations. Their characteristic equation was also quadratic, and one of the roots becomes unstable when $\Gamma = V\eta/(GR)$ is greater than a certain critical value. A similar instability was predicted in [3] for the case of Hagen–Poiseuille flow in a tube with deformable walls. The physical mechanism driving this instability was interpreted in terms of a transfer of energy from the mean flow to fluctuations through the deformation work done by the mean flow at the interface. Recently, Gkanis and Kumar [15] have interpreted the mechanism in terms of phase relationships between velocity and interfacial perturbations. At the critical conditions, they have shown that the mean flow tends to amplify horizontal perturbations to the interface location, while horizontal velocity perturbations in the fluid tend to suppress them. Predictions of KFP [2] were tested experimentally by Kumaran and Muralikrishnan [4], who used silicone oil on top of a polyacrylamide gel sheet in a parallel-plate

rheometer. A sharp increase in the apparent viscosity was observed above a critical strain rate, and this critical value was found to be in good agreement with the theoretical predictions [2] for onset of the instability.

If we consider the stability of a viscoelastic fluid past a deformable wall, we can anticipate additional time dependence in the problem due to the constitutive relation, and this could in principle lead to additional instabilities. This provides the second motivation for the present study: does the presence of elasticity in the fluid give rise to qualitatively new instabilities in the stability of plane Couette flow past a deformable surface? To answer these questions, we undertake a temporal linear stability analysis of the Couette flow of a UCM fluid past a linear viscoelastic solid in the creeping-flow regime.

There have been a number of studies which have analyzed the stability of the interface in two-layer Couette flow of UCM fluids (see, for example [16,17] and references therein), and it is pertinent here to contrast the present study with this previous literature. Renardy [16] analyzed the stability using an asymptotic analysis in the shortwave limit, and found that an elasticity difference between the two fluids could destabilize the flow even in the absence of a viscosity difference. The elasticity contrast between the two fluids results in a jump in the in the first normal stress difference across the two-fluid interface, and this jump produces an extra term in the shear stress continuity condition in the linear stability analysis, which was found to be the destabilizing agent in the absence of a viscosity difference. Chen [17] analyzed the complementary asymptotic limit of long waves, and again showed that a mere elasticity stratification is sufficient to induce the longwave instability, even if the viscosities of the two fluids are the same. In both [16] and [17], the leading order wavespeed in their respective asymptotic expansions is real (i.e., neutrally stable) and is identical to the corresponding two-layer Newtonian fluid problem, while the first correction (which determines the stability) scales as $1/k$ in the high-wavenumber expansion of Renardy [16], and as k in the low-wavenumber expansion of Chen [17]. While the present work shares some similarities with those studies in the formulation of the stability problem, it differs from the previous studies on two-layer Couette flow of UCM fluids in that the most unstable modes in the present study have finite wavenumber, and hence the present results cannot be captured by an asymptotic expansion (low or high) in the wavenumber. The wavespeed obtained from our analysis has both real and imaginary parts in the creeping-flow limit, regardless of the wavenumber, except when there is a transition from stable to unstable modes when flow then becomes neutrally stable.

The rest of this paper is organized as follows. In Section 2, the governing equations and boundary conditions are discussed, base state solutions are derived, and the linearized equations are developed along with analytical solutions for the eigenfunctions in the fluid and the wall. In Section 3, the results obtained from the stability analysis are discussed, and a summary of parameter values for which the flow is unstable is presented. To address the issue of nonlinear elasticity of the solid medium, we compare in Section 3.4 the results obtained for the linear elastic model with those obtained using a neo-Hookean model. Finally, the salient conclusions of the present study are discussed in Section 4.

2. Problem formulation

2.1. Governing equations

The system we consider consists of a linear viscoelastic solid of thickness HR and shear modulus G fixed onto a rigid surface at $z^* = -HR$, and a layer of viscoelastic fluid of thickness R in the region $0 < z^* < R$ (see Fig. 1). The viscoelastic fluid is modeled using the UCM model (see, for example [18]),

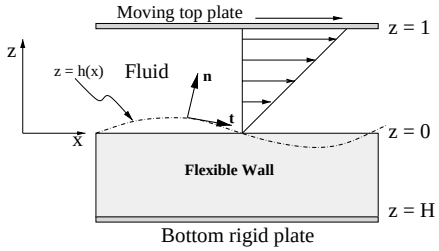

Fig. 1. Schematic diagram showing the configuration and coordinate system considered in Section 2.

which has two material constants: a viscosity η and a relaxation time τ_R. In what follows, we indicate dimensional variables with a superscript '$*$', and nondimensional variables without any superscript. The fluid is bounded at $z^* = R$ by a solid wall which moves at a constant velocity V in the x-direction relative to the deformable solid wall. It is useful to nondimensionalise various physical quantities at the outset, and the following scales are used for this purpose: R for lengths and displacements, V for velocities, R/V for time, and $\eta V/R$ for stresses and pressure. H, therefore, is the nondimensional thickness of the wall medium.

The nondimensional equations governing the dynamics of the fluid in the creeping-flow limit are respectively the continuity and momentum conservation equations:

$$\partial_i v_i = 0, \qquad \partial_j T_{ij} = 0. \tag{1}$$

Here, v_i is the velocity field in the fluid, and T_{ij} is the total stress tensor in the fluid which is a sum of an isotropic pressure $-p_f\delta_{ij}$ and the extra-stress tensor τ_{ij}:

$$T_{ij} = -p_f\delta_{ij} + \tau_{ij}, \tag{2}$$

and the indices i, j take the values x, z. The extra-stress tensor is prescribed by the UCM model as:

$$W[\partial_t\tau_{ij} + v_k\partial_k\tau_{ij} - \partial_k v_i\tau_{kj} - \partial_k v_j\tau_{ki}] + \tau_{ij} = (\partial_i v_j + \partial_j v_i), \tag{3}$$

where $\partial_t \equiv (\partial/\partial t)$, $\partial_i \equiv (\partial/\partial x_i)$, and $W = \tau_R V/R$ is the Weissenberg number which represents the ratio of the relaxation time of the viscoelastic fluid to the timescale for convective motions in the fluid. The Newtonian fluid is obtained in the limit $W \to 0$. No-slip boundary conditions are appropriate for the fluid at $z = 1$:

$$v_i = 0, \quad i = x, z \tag{4}$$

while the boundary conditions at the interface between the UCM fluid and the deformable wall are the continuity of velocity and stress, which are discussed a little later.

The deformable wall is modeled as an incompressible linear viscoelastic solid, similar to that used in the previous studies in this area (see, for example [3,6,7]). A recent study by Gkanis and Kumar [15] has examined the role of nonlinear rheological properties in the solid by modeling the deformable wall as a neo-Hookean solid, and this study shows that for nonzero interfacial tension and sufficiently large values of wall thickness, the results from both linear and nonlinear solid models agree quite well, while for small values of wall thickness, the linear model somewhat overpredicts the critical velocity required for destabilizing the flow. They also predict a shortwave instability in the absence of interfacial tension at the solid-fluid interface, and this was attributed to the nonzero first normal stress difference in the neo-Hookean solid. In

this work, we primarily restrict ourselves to a linear viscoelastic solid model, which allows us to focus on normal-stress phenomena that arise in the fluid. However, in order to demonstrate the validity of the results obtained, we also compare in Section 3.4 our results with those obtained using a neo-Hookean solid. The wall medium is described by a displacement field u_i, which represents the displacement of the material points in the medium from their steady-state positions. The velocity field in the wall medium is $v_i = \partial_t u_i$. In an incompressible linear viscoelastic solid, the displacement field satisfies the continuity equation:

$$\partial_i u_i = 0. \tag{5}$$

The momentum conservation equation, in the limit where the inertial stresses in the wall medium are negligible, is given by:

$$\partial_j \Sigma_{ij} = 0, \tag{6}$$

where $\Sigma_{ij} = -p_g \delta_{ij} + \sigma_{ij}$ is the total stress tensor which is given by a sum of the isotropic pressure p_g and deviatoric stress σ_{ij}. Note that the neglect of inertial stresses in the solid assumes that the density of the wall medium is comparable to the density of the fluid. For example, this is a reasonable assumption for deformable walls made up of aqueous polymer gels where the densities of the fluid and the gel are comparable. The deviatoric stress tensor σ_{ij} is given by a sum of elastic and viscous stresses in the wall:

$$\Sigma_{ij} = \left(\frac{1}{\Gamma} + \eta_r \partial_t \right) (\partial_i u_j + \partial_j u_i), \tag{7}$$

where $\Gamma = V\eta/(GR)$ is the nondimensional quantity characterizing the elasticity of the deformable wall and η_r is the ratio of wall to fluid viscosities η_w/η. More precisely, $1/\Gamma$ is the estimated ratio of elastic stresses in the wall to viscous stresses in the UCM fluid. The nondimensional group Γ can also be interpreted as the nondimensional velocity of the top plate, as was done in [2]. The wall is assumed to be fixed to a rigid surface at $z = -H$, and the boundary condition for the displacement field there is $u_i = 0$.

The boundary conditions at the interface $z = h(x)$ between the UCM fluid and the deformable wall are the continuity of the velocities and stresses:

$$v_i = \partial_t u_i, \qquad T_{ij} n_j = \Sigma_{ij} n_j, \tag{8}$$

where n_j is the unit normal to the interface $z = h(x)$ between the fluid and the wall (see Fig. 1). The normal and tangential stress continuity conditions at the interface are obtained by contracting the second equation in Eq. (8) with the unit normal and tangential vectors n_i and t_i respectively:

$$-p_f + n_i \tau_{ij} n_j = -p_g + n_i \sigma_{ij} n_j, \tag{9}$$

$$t_i \tau_{ij} n_j = t_i \sigma_{ij} n_j. \tag{10}$$

We neglect the effect of interfacial tension in the normal stress continuity condition (Eq. (9)), as this was found to have a purely stabilizing effect on the instability in the earlier study of KFP [2].

2.2. Base state

The steady, unidirectional, x-independent base state whose stability is of interest in the present study is easily obtained by solving the momentum equations in the fluid and the wall. We look for a steady solution in which the fluid-wall interface is uniform and flat, and so the unit normal to the interface is

given by $n_x = 0, n_z = 1$, and similarly for the unit tangent $t_x = 1, t_z = 0$. The displacement and stress fields in the wall are obtained by using the tangential stress continuity condition (10) with the above values for n_i and t_i. After using the boundary conditions at $z = 1$ and $z = -H$, we obtain for the fluid:

$$\bar{v}_x = z, \qquad \bar{v}_z = 0, \qquad \bar{\tau}_{xx} = 2W, \qquad \bar{\tau}_{zz} = 0, \qquad \bar{\tau}_{xz} = \bar{\tau}_{zx} = 1, \tag{11}$$

and for the wall:

$$\bar{u}_x = \Gamma(z + H), \qquad \bar{u}_z = 0, \qquad \bar{\sigma}_{xx} = 0, \qquad \bar{\sigma}_{zz} = 0, \qquad \bar{\sigma}_{xz} = \bar{\sigma}_{zx} = 1. \tag{12}$$

All the base flow quantities above are denoted with an overbar in the following discussion. The steady velocity profile is simply the Couette flow profile, identical to that found for Newtonian fluids. Note, however, that there is a nonzero first normal stress difference $\bar{\tau}_{xx} - \bar{\tau}_{zz} = 2W$ which vanishes in the case of Newtonian fluids ($W = 0$). The wall is at rest in this steady base state, but there is a nonzero unidirectional displacement $\bar{u}_x$ due to the fluid shear stresses at the interface. The base state displacement gradient (or the strain) in the solid medium is Γ. The linear elastic solid model, strictly speaking, is formally valid only when $\Gamma \ll 1$. We nonetheless consider the effect of increasing Γ to O(1) on the stability of the fluid. We later demonstrate in Section 3.4 that the linear elastic model gives rise to accurate predictions even when Γ is not truly small compared to 1 (provided $H \geq 2$), by comparing the results for the linear elastic model with those for a neo-Hookean model.

2.3. Linear stability analysis

Small perturbations are introduced to the fluid velocity about the base state, $v_i = \bar{v}_i + v_i'$, and other dynamical quantities in the fluid and the wall are similarly perturbed. Carrying out linearizion for the interface conditions (Eq. (8)) involves performing a Taylor-series expansion about the unperturbed interface location and yields the following linearized conditions to be applied at $z = 0$:

$$v_z' = \partial_t u_z', \tag{13}$$

$$v_x' + u_z' = \partial_t u_x', \tag{14}$$

$$-p_\mathrm{f}' + \tau_{zz}' = -p_\mathrm{g}' + \sigma_{zz}', \tag{15}$$

$$\tau_{xz}' - \frac{\partial u_z'}{\partial x}(2W) = \sigma_{xz}'. \tag{16}$$

Here, the second term in the left side of Eqs. (14) and (16) represent nontrivial contributions that arise as a result of the Taylor expansion of the mean flow quantities about the unperturbed interface. The term in (14) arises due to the discontinuity in the gradient of the base flow velocity profile at the interface, while the term in (16) arises due to the discontinuity of the first normal stress difference between the fluid and the wall medium. The presence of such a term in the tangential stress interface condition (Eq. (16)) was clearly pointed out by Chen [17] and was also correctly incorporated by Renardy [16] in their studies of two-layer Couette flow of UCM fluids.

We use a temporal stability analysis to determine the fate of small perturbations to the above base state. All the perturbation quantities (denoted by a prime in the above discussion) are expanded in the form of spatially periodic Fourier modes in the x-direction, and with an exponential dependence on time:

$$v_i' = \tilde{v}_i(z)\exp[\mathrm{i}k(x - ct)], \qquad u_i' = \tilde{u}_i(z)\exp[\mathrm{i}k(x - ct)], \tag{17}$$

where k is the wavenumber, c is the wavespeed which is a complex number, and $\tilde{v}_i(z)$ and $\tilde{u}_i(z)$ are eigenfunctions which are determined below from the linearized governing equations and boundary conditions. For simplicity, only two-dimensional perturbations are considered. The complex wavespeed is $c = c_\mathrm{r} + \mathrm{i}c_\mathrm{i}$, and when $c_\mathrm{i} > 0$, the base state is temporally unstable and small fluctuations grow exponentially with time. We note that transient (nonexponential) growth phenomena in Couette flow of a UCM fluid in a rigid channel have been considered by Sureshkumar et al. [19], but here we focus only on exponentially growing or decaying disturbances that can be decomposed to normal modes.

Upon substituting the above form for the perturbations in the governing equations for the fluid (1) and the constitutive relation for the UCM fluid (3), we obtain the following linearized equations governing the eigenfunctions, where $\mathrm{d}_z = \mathrm{d}/\mathrm{d}z$:

$$\mathrm{d}_z\tilde{v}_z + \mathrm{i}k\tilde{v}_x = 0, \tag{18}$$

$$-\mathrm{i}k\tilde{p}_\mathrm{f} + \mathrm{i}k\tilde{\tau}_{xx} + \mathrm{d}_z\tilde{\tau}_{xz} = 0, \tag{19}$$

$$-\mathrm{d}_z\tilde{p}_\mathrm{f} + \mathrm{d}_z\tilde{\tau}_{zz} + \mathrm{i}k\tilde{\tau}_{xz} = 0, \tag{20}$$

$$\{1 + \mathrm{i}kW(z-c)\}\tilde{\tau}_{zz} = 2\mathrm{d}_z\tilde{v}_z + 2\mathrm{i}kW\tilde{v}_z, \tag{21}$$

$$\{1 + \mathrm{i}kW(z-c)\}\tilde{\tau}_{xz} = (\mathrm{d}_z\tilde{v}_x + \mathrm{i}k\tilde{v}_z) + W(\tilde{\tau}_{zz} + 2\mathrm{i}kW\tilde{v}_z), \tag{22}$$

$$\{1 + \mathrm{i}kW(z-c)\}\tilde{\tau}_{xx} = 2\mathrm{i}k\tilde{v}_x + W(2\tilde{\tau}_{xz} + 4\mathrm{i}kW\tilde{v}_x + 2\mathrm{d}_z\tilde{v}_x). \tag{23}$$

To obtain a single fourth-order ordinary differential equation for $\tilde{v}_z$, similar to the Orr–Sommerfeld equation for Newtonian fluids, we can differentiate Eq. (19) with respect to z and multiply Eq. (20) by $(-\mathrm{i}k)$ and add the resulting equations to obtain:

$$(\mathrm{d}_z^2 + k^2)\tilde{\tau}_{xz} + \mathrm{i}k\mathrm{d}_z(\tilde{\tau}_{xx} - \tilde{\tau}_{zz}) = 0. \tag{24}$$

This can be reduced to a single fourth-order equation for $\tilde{v}_z$ after using the Eqs. (18), (21)–(23), following G–L [9]:

$$\{\xi^2\mathrm{d}_z^2 - 2\xi\mathrm{d}_z + 2 - k^2\xi^2\}\{\mathrm{d}_z^2 + 2\mathrm{i}kW\mathrm{d}_z - k^2 - 2k^2W^2\}\tilde{v}_z = 0, \tag{25}$$

where the variable ξ is defined as $\xi = [z - c - \mathrm{i}/(kW)]$.

The governing equations for the displacement field in the wall can be expressed in terms of $\tilde{u}_i(z)$ in a similar manner to give:

$$\mathrm{d}_z\tilde{u}_z + \mathrm{i}k\tilde{u}_x = 0, \tag{26}$$

$$-\mathrm{i}k\tilde{p}_\mathrm{g} + \left(\frac{1}{\Gamma} - \mathrm{i}kc\eta_\mathrm{r}\right)(\mathrm{d}_z^2 - k^2)\tilde{u}_x = 0, \tag{27}$$

$$-\mathrm{d}_z\tilde{p}_\mathrm{g} + \left(\frac{1}{\Gamma} - \mathrm{i}kc\eta_\mathrm{r}\right)(\mathrm{d}_z^2 - k^2)\tilde{u}_z = 0. \tag{28}$$

These equations can be reduced to a single fourth-order differential equation for $\tilde{u}_z$:

$$(\mathrm{d}_z^2 - k^2)(\mathrm{d}_z^2 - k^2)\tilde{u}_z = 0. \tag{29}$$

The linearized boundary conditions at the unperturbed interface position $z = 0$ are given by:

$$\tilde{v}_z = (-\mathrm{i}kc)\tilde{u}_z, \tag{30}$$

$$\tilde{v}_x + \tilde{u}_z = (-\mathrm{i}kc)\tilde{u}_x, \tag{31}$$

$$-\tilde{p}_\mathrm{f} + \tilde{\tau}_{zz} = -\tilde{p}_\mathrm{g} + \frac{1}{\Gamma}2\mathrm{d}_z\tilde{u}_z - 2\mathrm{i}kc\eta_\mathrm{r}\mathrm{d}_z\tilde{u}_z, \tag{32}$$

$$\tilde{\tau}_{xz} - 2\mathrm{i}kW\tilde{u}_z = \left(\frac{1}{\Gamma} - \mathrm{i}kc\eta_\mathrm{r}\right)(\mathrm{d}_z\tilde{u}_x + \mathrm{i}k\tilde{u}_z). \tag{33}$$

The boundary conditions at $z = 1$ are simply $\tilde{v}_z = 0$ and $\tilde{v}_x = 0$, while the boundary conditions at $z = -H$ are $\tilde{u}_z = 0$ and $\tilde{u}_x = 0$.

The general solution to the fourth-order differential equation governing the stability of the fluid (25) can be obtained analytically [9]:

$$\begin{aligned}\tilde{v}_z = {} & A_1(z-c)\exp[kz] + A_2(z-c)\exp[-kz] + A_3\exp[k(-\mathrm{i}W + \sqrt{1+W^2})z] \\ & + A_4\exp[-k(\mathrm{i}W + \sqrt{1+W^2})z].\end{aligned} \tag{34}$$

The coefficients $\{A_1 \cdots A_4\}$ multiplying the four linearly independent solutions are determined from the boundary conditions at $z = 1$ and the interface conditions (30)–(33) at $z = 0$. The most general solution to the fourth-order differential equation governing the wall, (29), has four linearly independent solutions and four coefficients multiplying these solutions. Two of the coefficients can be expressed in terms of the other two after using the zero displacement conditions ($\tilde{u}_z = 0$, $\tilde{u}_x = 0$) at $z = -H$, and we obtain:

$$\begin{aligned}\tilde{u}_z = {} & B_1\{\exp[kz] - [1 + 2k(z+H)]\exp[-2Hk - kz]\} + B_2\{kz\exp[kz] \\ & + [k(2Hk(z+H) - z)]\exp[-2Hk - kz]\}.\end{aligned} \tag{35}$$

The eigenfunctions for the x-component of the velocity field and pressure in the fluid are obtained respectively from the continuity Eq. (18) and the x-momentum Eq. (19), while the eigenfunctions for the various components of the stress tensor in the fluid are obtained from Eqs. (21)–(23). Similarly, the expressions for $\tilde{u}_x$ and pressure field $\tilde{p}_\mathrm{g}$ in the wall medium are obtained respectively from Eqs. (26) and (27). The solution for the fluid velocity (34) and pressure fields and the wall displacement (35) and pressure fields are then inserted into the conditions at the interface, (30)–(33), and the boundary conditions at $z = 1$, viz., $\tilde{v}_z = 0$, $\tilde{v}_x = 0$, to obtain the characteristic matrix of the form:

$$\boldsymbol{M} \cdot \boldsymbol{C}^\mathrm{T} = 0, \tag{36}$$

where $\boldsymbol{C}$ is the vector of coefficients

$$\boldsymbol{C} = [A_1, A_2, A_3, A_4, B_1, B_2], \tag{37}$$

and $\boldsymbol{M}$ is a 6×6 matrix in which the six rows are obtained from the four conditions at the interface and two conditions at $z = 1$. The characteristic equation is obtained by setting the determinant of the characteristic matrix $\boldsymbol{M}$ to zero. The characteristic equation thus obtained in the most general case where $\Gamma \neq 0$ and $W \neq 0$ is a sixth order polynomial in c, and so has six roots. When $W = 0$ and $\Gamma \neq 0$, we recover the quadratic characteristic equation obtained by KFP [2] for Newtonian fluids, and when $\Gamma = 0$ and $W \neq 0$, we recover the quadratic characteristic equation obtained by G–L [9] for the case of UCM fluids flowing past a rigid

surface. The solution of the characteristic equation gives the wavespeed c as a function of the wavenumber k for different values of Γ, W, H and η_r. The effect of changes in the various parameter values on the wavespeed and the neutral stability curves are discussed in the following section. The stability calculations were performed using Mathematica, and where convenient, a Fortran code was used to generate the results.

3. Results

3.1. Effect of wall elasticity on G–L modes

We first discuss the effect of wall elasticity on the modes obtained by G–L [9], and it is useful to recall their results first. In their study on the linear stability of Couette flow of UCM fluid in a rigid channel, they obtained a quadratic characteristic equation for the wavespeed c in the creeping-flow limit, and the roots of the equation indicated that the Couette flow of the UCM fluid is always *stable* in this limit. In addition to the two discrete modes, there exists also a continuous spectrum of modes (also see [10,11]), which are obtained by equating the coefficient of the term with the highest derivative in the governing stability Eq. (25) to zero, which yields $c_i = -1/(kW)$, and c_r can take continuous values between 0 and 1 (the nondimensional velocity of the top plate). This shows that the continuous spectrum of modes is always stable, and is not affected by wall elasticity, which enters only through the interface conditions. Therefore, in the following discussion, we restrict our attention to the two discrete stable modes predicted by G–L [9]. We note that for a rigid wall, the elastic stresses in the wall are very large compared to the fluid viscous stresses, and thus $\Gamma = 0$.

The effect of increasing Γ on c_i and c_r of the two (discrete) G–L modes is shown in Figs. 2 and 3, for fixed values of k, W, H and η_r. At $\Gamma = 0$, both the modes have the same c_i (i.e., the same growth rate) which is negative, but different values of c_r. For $\Gamma < 10^{-4}$, the c_i for both the modes remain the same, but when $\Gamma > 10^{-4}$ the c_i for the two modes start differing. For sufficiently high values of Γ, one of the modes becomes unstable while the other mode remains stable. The other four roots of the characteristic equation also remain stable upon increasing Γ. This trend is found to be true for other parameter values as well: for a fixed value of W, the Couette flow of UCM fluid past a deformable wall becomes linearly unstable for sufficiently high values of Γ, i.e., when the wall becomes sufficiently deformable. Thus, wall deformability has a destabilizing effect on the stable G–L modes.

In the rigid limit ($\Gamma = 0$), the parameters characterizing the wall such as H and η_r do not have any influence on the stable G–L modes. However, it is expected that these parameters should affect the stability as Γ is increased. The effect of increasing Γ on the G–L mode (that becomes unstable at finite Γ) for two different values of H is shown in Fig. 4 (c_r versus Γ) and Fig. 5 (c_i versus Γ). These figures show that for very low values of Γ ($< 10^{-7}$), there is no effect of H and both the $H = 1$ and $H = 10$ modes have the same c_r and c_i values, while for higher values of Γ($> 10^{-7}$), the mode for $H = 10$ starts deviating first from its rigid wall value. For values of $\Gamma > 10^{-5}$, the mode for $H = 1$ also deviates from its rigid wall value. One way to rationalize the result that the $H = 10$ mode starts deviating first is as follows: for a given value of Γ, the wall with a lower (higher) thickness is more rigid (deformable) because the resistance of the bottom rigid plate at $z = -H$ is increasingly felt by the fluid as the solid thickness decreases. Therefore, the effect of wall deformability is felt on the $H = 10$ mode even at very small values of Γ, when compared to the $H = 1$ mode. The results of Figs. 4 and 5 show that different modes which exist due to varying degree of wall deformability merge to give the same value as that of the rigid G–L mode as $\Gamma \to 0$.

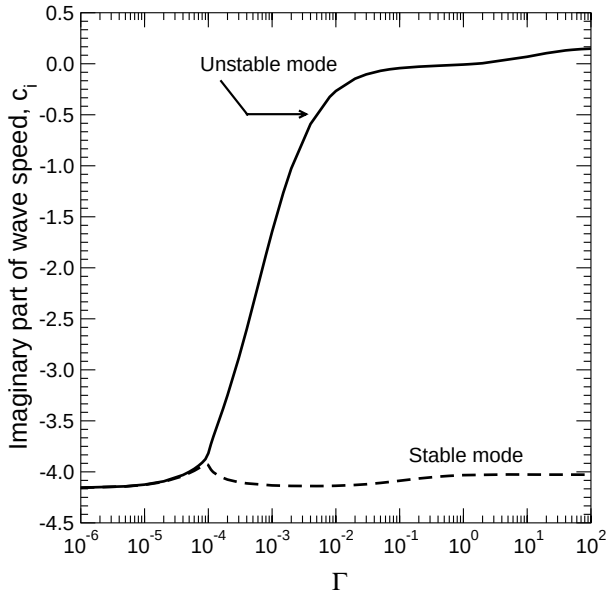

Fig. 2. Effect of wall deformability on the G–L modes: imaginary part of c as a function of Γ for $W = 20$, $H = 20$, $k = 0.012$, $\eta_r = 0$.

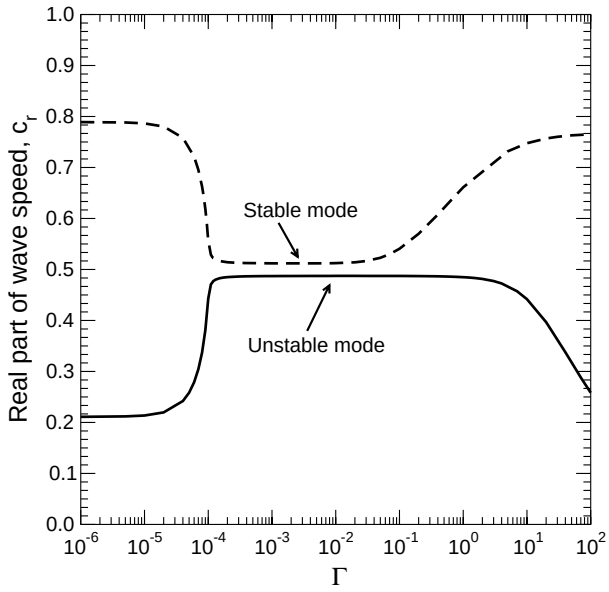

Fig. 3. Effect of wall deformability on the G–L modes: real part of c as a function of Γ for $W = 20$, $H = 20$, $k = 0.012$, $\eta_r = 0$.

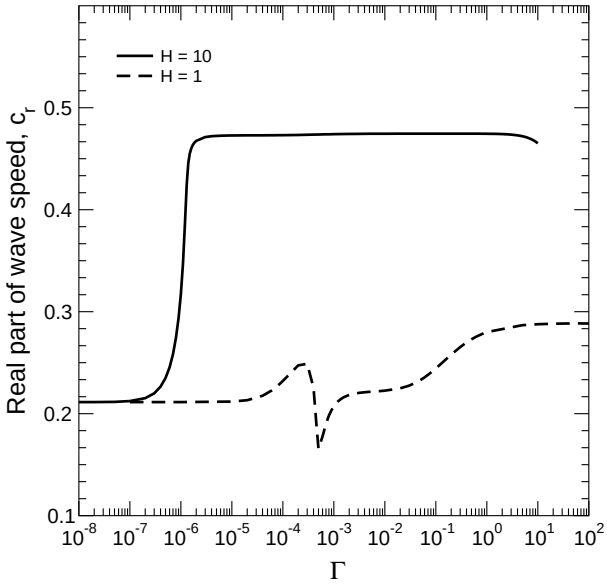

Fig. 4. Effect of wall deformability on the G–L modes for two different values of H: c_r as a function of Γ for $W = 1$, $k = 0.01$, $\eta_r = 0$.

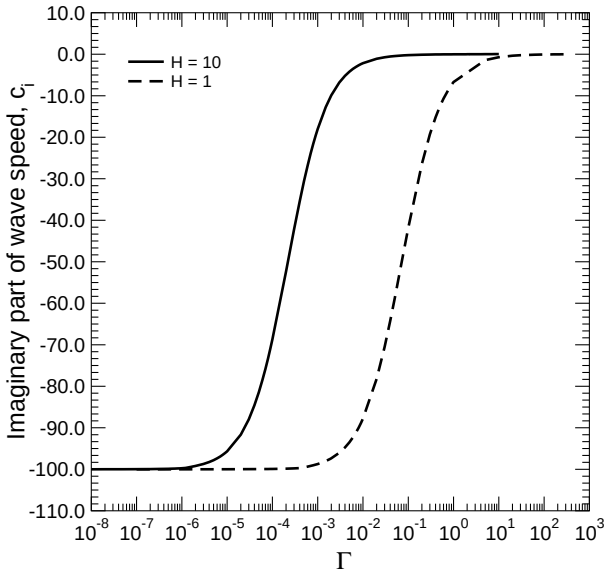

Fig. 5. Effect of wall deformability on the G–L modes for two different values of H: c_i as a function of Γ for $W = 1$, $k = 0.01$, $\eta_r = 0$.

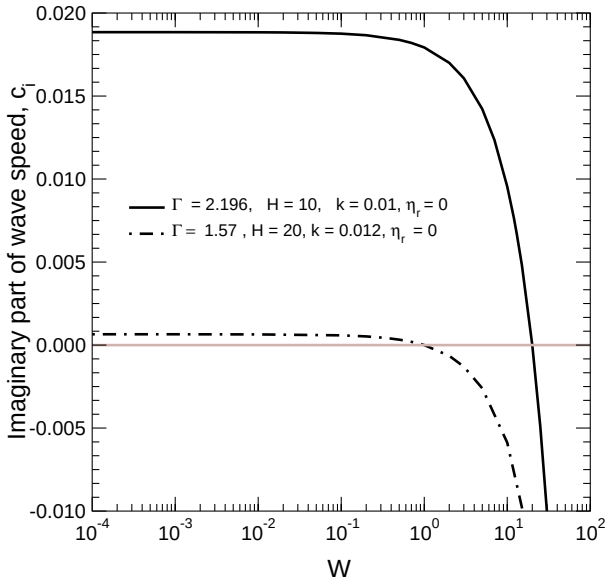

Fig. 6. Effect of finite fluid elasticity on the KFP modes: c_i as a function of W.

3.2. *Effect of fluid elasticity on KFP modes*

We next turn to the effect of nonzero W, i.e., finite elasticity effects in the fluid, on the unstable modes reported by KFP [2] for the stability of Couette flow of a Newtonian fluid past a deformable wall. Fig. 6 shows the effect of increasing W on c_i for the unstable KFP modes for two different sets of parameters, and this shows that at finite W the unstable KFP modes are stabilized. This trend is found to be true for a variety of parameter sets. Thus, elastic effects in the fluid have a stabilizing effect on the KFP instability. The fact that wall elasticity has a destabilizing effect on the G–L modes while fluid elasticity has a stabilizing effect on the KFP modes raises the question as to whether these modes are similar at finite values of wall and fluid elasticity. In particular, is the continuation of the G–L mode (that becomes unstable) to finite Γ at fixed W identical to the continuation of KFP modes at fixed Γ and finite W? This indeed turns out to be true for all the parameter values explored.

An example of this 'merging' of G–L and KFP modes at finite W and Γ is shown in Tables 1 and 2. Table 1 shows the continuation of the stable G–L mode to finite wall elasticity for $W = 20$, until the flow becomes neutrally stable, i.e., $c_i = 0$. For the data shown in Table 2, Γ is fixed at the value for which $c_i = 0$ in Table 1, and W is increased from zero to finite values. For this fixed value of Γ, when $W = 0$, the flow is unstable ($c_i > 0$), indicating that this mode corresponds to the unstable KFP mode for Newtonian fluids. Upon increasing W to 20 and keeping Γ fixed, we find that $c_i = 0$ and c_r is the same as in Table 1. These data thus show that the continuation of the G–L mode that becomes unstable at finite Γ merges with the continuation of the KFP modes at finite W. One of the motivations for undertaking the present analysis was to determine if the stable G–L modes give rise to *new* unstable modes as Γ increases. But the picture that emerges from the analysis is rather simple: in the creeping-flow limit, there is just one unstable mode at finite W and Γ (for fixed values of k, H, η_r) which reduces to the stable G–L mode as $\Gamma \to 0$, and to the unstable KFP mode as $W \to 0$. This is one of the main results of the present study.

Table 1
Continuation of G–L modes to finite Γ: c_r and c_i as a function of Γ for $W = 20$, $H = 20$, $k = 0.012$, $\eta_r = 0$

Γ	c_r	c_i
1E−06	0.210988441	−4.1552864
1E−05	0.213588778	−4.12520545
5E−05	0.258348017	−4.00030786
7E−05	0.304346927	−3.94080264
8E−05	0.336877972	−3.9102796
9E−05	0.380896928	−3.87605665
0.0001	0.442793673	−3.81820393
0.00011	0.470530748	−3.72815966
0.00013	0.480070422	−3.59169642
0.00015	0.482765716	−3.48063524
0.00017	0.484037691	−3.38200356
0.0002	0.485029682	−3.24899406
0.0003	0.486186854	−2.88556821
0.0004	0.48655442	−2.60127503
0.0006	0.486839157	−2.17724972
0.0008	0.486963904	−1.87398279
0.001	0.487037684	−1.64575684
0.0015	0.487140992	−1.26334123
0.002	0.487197884	−1.02652848
0.004	0.487295091	−0.590815819
0.008	0.487348026	−0.325142268
0.01	0.487357361	−0.267255007
0.03	0.487354886	−0.103936514
0.05	0.487322091	−0.0694346529
0.07	0.487284294	−0.0543245468
0.1	0.487224119	−0.0427277883
0.8	0.485479741	−0.0108165401
1	0.484887607	−0.00771311915
1.5	0.483249636	−0.000898232543
1.57068819	0.483001248	9.90286765E−12

The wavespeed obtained for truly rigid walls ($\Gamma = 0$) in the G–L analysis is: $c_r = 0.210881$ and $c_i = -4.15834204$.

It is appropriate here to remark on the relevance of the present instability to Oldroyd-B fluids. Wilson et al. [10] have shown that the addition of solvent viscosity to the polymer stress increases the complexity of the eigenspectrum for Couette flow of Oldroyd-B fluids in a rigid channel: in addition to the continuous spectrum and the two discrete G–L modes that exist for the UCM model, there is a string of (stable) discrete eigenvalues which appear in the Oldroyd-B model, and the number of these discrete eigenvalues was found to increase indefinitely as the ratio of solvent to the total (solvent + polymer) viscosity approaches zero. Thus, the stability results for Oldroyd-B show that the two G–L discrete (UCM) eigenvalues are preserved in the case of Oldroyd-B as well. Hence, the present results, which can be interpreted as a continuation of the G–L modes to finite wall deformability, are expected to be valid for the stability of an Oldroyd-B fluid past a deformable wall. The effect of wall deformability on the other (stable) discrete modes found for the Oldroyd-B model cannot be addressed in this work and will be the subject of a future study.

Table 2
Continuation of KFP modes to finite W: c_r and c_i as a function of W for $\Gamma = 1.57068819$, $H = 20$, $k = 0.012$, $\eta_r = 0$

W	c_r	c_i
0.0001	0.485734923	0.0188475259
0.001	0.485734792	0.0188466948
0.01	0.485733485	0.0188383836
0.1	0.485720413	0.0187552683
0.5	0.48566242	0.0183857931
1	0.485590169	0.0179237662
5	0.485021303	0.0142176921
10	0.484330757	0.0095480015
15	0.483658983	0.0048163671
20	0.483001248	9.60799782E−12

The wavespeed obtained in the KFP analysis with $W = 0$ is: $c_r = 0.485735$, $c_i = 0.0188476$.

3.3. Neutral stability and critical parameters

Having established that there is just one unstable mode at finite W and Γ in the creeping-flow limit, we now turn to study in detail the neutral stability curves and the critical values of parameters such as Γ, H and η_r for which the instability exists for the UCM fluid. Fig. 7 presents a typical neutral stability curve ($c_i = 0$) in the $\Gamma - k$ plane at fixed values of W, H and η_r. This curve shows that the instability occurs only at finite wavenumbers, and the minimum value of Γ in this curve at which instability occurs is identified as Γ_c—the critical Γ required for instability at fixed values of H, W and η_r, and the wavenumber at which this minimum occurs is identified as k_c, the critical wavenumber. This critical wavenumber is

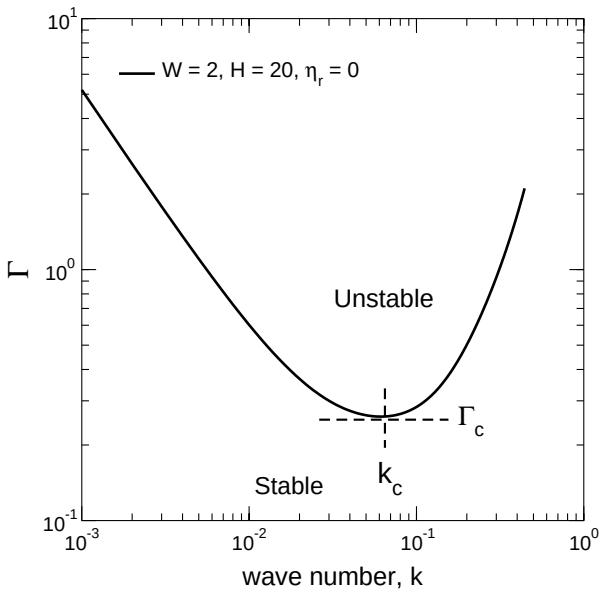

Fig. 7. Neutral stability curve: Γ vs. k for $H = 20$, $W = 2$, $\eta_r = 0$.

generally found to be an O(1) quantity, indicating that the most unstable modes have finite wavelengths. Gkanis and Kumar [15] studied the stability of Couette flow of a Newtonian fluid past a neo-Hookean solid, and showed that the jump in the first normal stress difference across the solid-fluid interface in the base state gave rise to a shortwave instability at high k, when the interfacial tension was zero. Similarly, the earlier work of Renardy [16] which studied the two-layer Couette flow of UCM fluids, also found a shortwave instability due to the jump in the first normal stress difference in the base state. In the present study, however, the jump in the first normal stress difference across UCM fluid—linear viscoelastic solid interface in the base state does not give rise to any shortwave instability. This indicates that shortwave instability requires using a model for the solid that properly accounts for large displacement gradients. The variation of Γ_c with W for various values of H is shown next in Fig. 8 for $\eta_r = 0$. This set of curves show that for $W < 1$, Γ_c approaches its Newtonian value as found in [2], while for $W \gg 1$, $\Gamma_c \propto W$. This shows that elasticity in the fluid has a stabilizing effect.

In Fig. 8, both $\Gamma = V\eta/(GR)$ and $W = \tau_R V/R$ have fluid velocity in their definition. It is more appropriate to plot the dependence of Γ_c (which is a nondimensional critical velocity of the top plate for instability to occur) on a flow independent quantity, and to this end we define $\bar{W} \equiv \tau_R G/\eta = W/\Gamma$. This flow-independent modified Weissenberg number $\bar{W}$ is the ratio of the relaxation time in the viscoelastic fluid τ_R to the viscous relaxation time of the wall dynamics η/G. This timescale η/G can be interpreted as the time taken for a surface fluctuation in the wall to decay in the absence of the fluid flow. Indeed, KFP [2] have used this cale η/G to nondimensionalise time from the outset of their calculation. However, in this study, we intend to recover the limiting case of a rigid wall to study the effect of wall elasticity on the G–L modes, and hence it was necessary to choose the convective timescale in the flow, R/V, in the beginning (the timescale η/G vanishes in the limit of large wall elasticity). Plotting Γ_c versus $\bar{W}$ thus allows one to easily demarcate the presence of unstable and stable regions in parameter space. In addition,

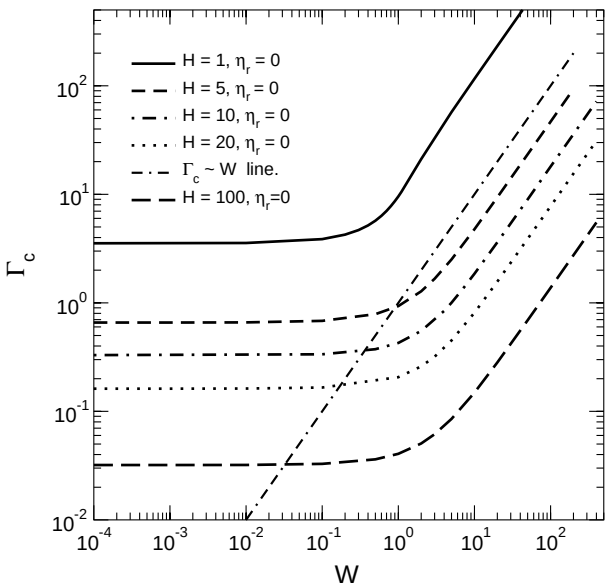

Fig. 8. Variation of Γ_c vs. W for different values of H and $\eta_r = 0$.

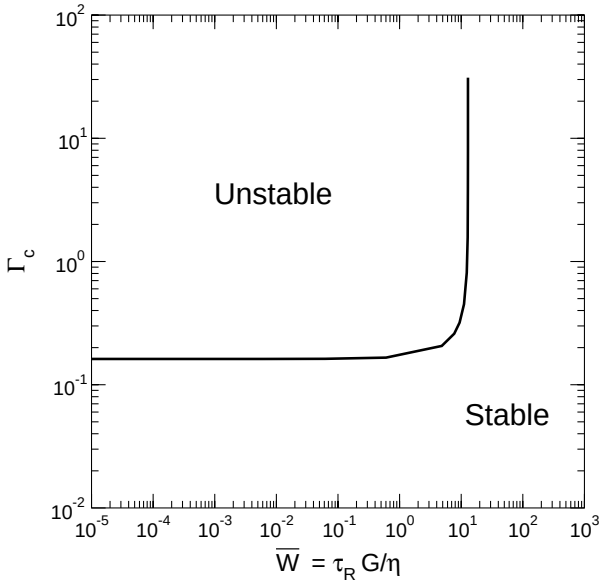

Fig. 9. Variation of Γ_c vs. $\bar{W}$ for $H = 20$ and $\eta_r = 0$.

it allows for connection with experiments in a simple way: by first choosing various material properties and geometric parameters, one can recover the *dimensional* critical velocity required for triggering the instability from the plot of Γ_c versus $\bar{W}$.

Fig. 9 shows the variation of Γ_c with the modified Weissenberg number $\bar{W}$ for $H = 20$ and $\eta_r = 0$, and this plot shows that until $\bar{W} \approx 1$, Γ_c has the value appropriate for a Newtonian fluid, while for $\bar{W} > 10^{-1}$, the instability ceases to exist as Γ_c increases rapidly at $\bar{W} \approx 10^{-1}$. Fig. 10 shows Γ_c versus $\bar{W}$ for various values of wall thickness, H, with $\eta_r = 0$. Interestingly, the Γ_c required to trigger the instability is nearly equal to its Newtonian value (defined as $\Gamma_{c,Newt}$; see Fig. 10) when the instability exists, and Γ_c increases very rapidly near a cut-off modified Weissenberg number $\bar{W}_{max}$ (see Fig. 10). Thus, the plot of Γ_c versus $\bar{W}$ gives rise to a 'rectangular' unstable zone in which two parameters are important: the limiting value of Γ_c above which instability exists, which is equal to its Newtonian limiting value, $\Gamma_{c,Newt}$, and the cut-off $\bar{W}$, denoted as $\bar{W}_{max}$, *above which instability ceases to exist*. As seen in this figure, $\Gamma_{c,Newt}$ decreases with increasing H, while $\bar{W}_{max}$ increases with increasing H, thus showing that the region of instability becomes larger as H increases. Fig. 11 shows the variation of the critical wavenumber, k_c, with $\bar{W}$. The critical wavenumber for instability of the UCM fluid at finite $\bar{W}$ is also very nearly equal to the critical wavenumber for a Newtonian fluid, when the instability exists. The critical wavenumber decreases rapidly at $\bar{W} = \bar{W}_{max}$, but the instability ceases to exist at this point. Thus, both Γ_c and k_c for the UCM fluid are approximately equal to the limiting Newtonian values when the instability exists for the UCM fluid, i.e., when $\bar{W} < \bar{W}_{max}$.

In order to describe the parameter space in which the Couette flow of a UCM fluid past a deformable wall is unstable, it therefore suffices to specify how $\Gamma_{c,Newt}$ and $\bar{W}_{max}$ vary with H and η_r. The variation of $\Gamma_{c,Newt}$ with H and η_r was already presented in the study of KFP [2] (see their Fig. 12). Therefore, it is sufficient to determine the variation of $\bar{W}_{max}$ with H for different values of η_r, and this is shown in

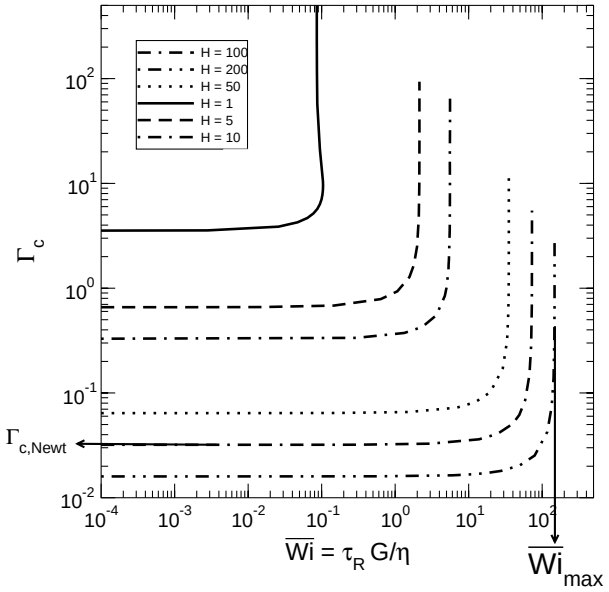

Fig. 10. Variation of Γ_c vs. $\bar{W}$ for different values of H and $\eta_r = 0$.

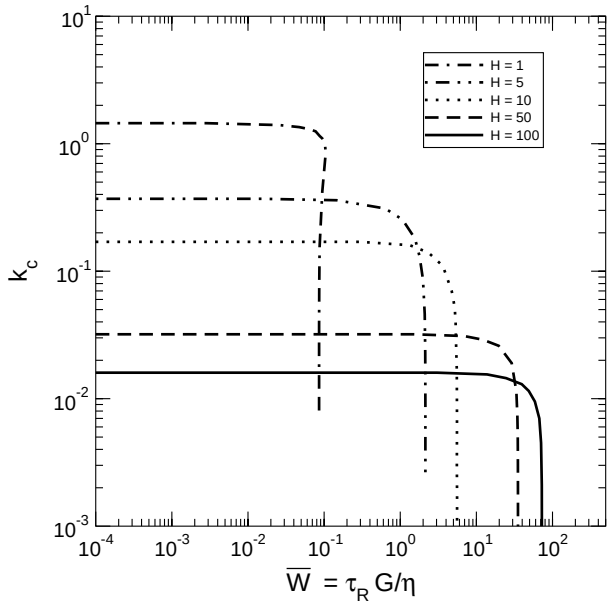

Fig. 11. Variation of k_c vs. $\bar{W}$ for different values of H and $\eta_r = 0$.

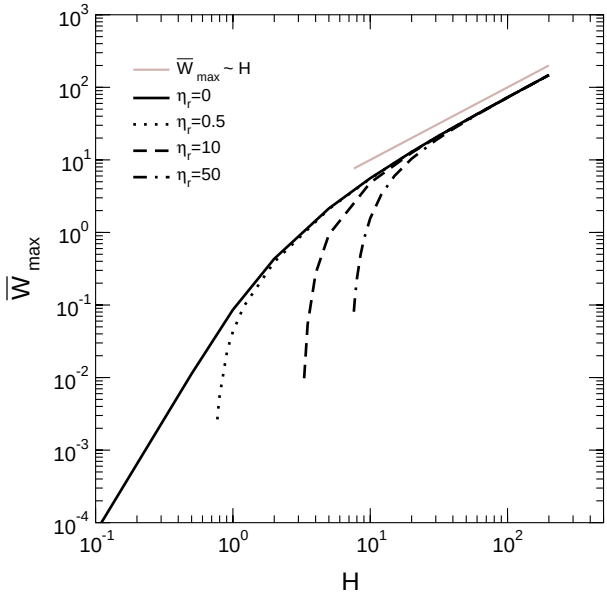

Fig. 12. Variation of $\bar{W}_{\max}$ with H for different η_r.

Fig. 12. These results indicate that for $\eta_r = 0$, and for $H < 1$, $\bar{W}_{\max} \propto H^3$, while for $H \gg 1$, $\bar{W}_{\max} \propto H$. For higher values of η_r however, $\bar{W}_{\max}$ decreases rapidly for smaller values of H, and the instability is nonexistent for the UCM fluid at $H < H_{\min}$, where $H_{\min}$ increases with an increase in η_r. For $H \gg 1$, the instability exists for the UCM fluid for any η_r, and $\bar{W}_{\max} \propto H$ for $H \gg 1$. In the same limit, the results of [2] indicated that for the case of Newtonian fluids, $\Gamma_{c,\mathrm{Newt}} \propto H^{-1}$. This suggests that, for $H \gg 1$, if we plot $\Gamma_{c,\mathrm{Newt}} H$ versus $\bar{W}/H$, the data for different values of H should collapse. This is indeed found to be the case, and this data collapse for large H is shown in Fig. 13 for $\eta_r = 0$. This figure shows that even a wall thickness of $H = 10$ is high enough to approach the $H \gg 1$ asymptotic regime and the data collapse is nearly perfect for higher values of H. The data for critical wavenumber as a function of $\bar{W}$ also show a collapse for $H \gg 1$ when plotted in terms of $k_c H$ versus $\bar{W}/H$, and this is shown in Fig. 14.

The reason for $\Gamma_{c,\mathrm{Newt}} \propto H^{-1}$ and $\bar{W} \propto H$ at $H \gg 1$ can be understood by a simple dimensional analysis of the tangential stress balance. The viscous stresses in the fluid can be estimated as $V\eta/R$, while the elastic stresses in the wall are nominally estimated as G, where it is implicitly assumed that the lengthscale for variation in the wall is R. However, in the limit $H \gg 1$, where the wall thickness is large compared to the fluid thickness, the correct estimate for elastic stresses in the wall is $G\partial u_x^*/\partial y^* \sim G/H$, since the lengthscale for variation is HR in the wall. Using this estimate for the elastic stress, when we balance the viscous stresses in the fluid and elastic stresses in the solid, we obtain $V\eta/R \sim G/H$, or, $\Gamma \sim 1/H$. Similarly, the modified Weissenberg number $\bar{W} = \tau_R G/\eta$ can be interpreted as the ratio of elastic stresses in the wall to elastic stresses in the viscoelastic fluid. Here again, for $H \gg 1$, if we estimate the elastic stress in the wall as G/H instead of G, we obtain, upon balancing the elastic stresses in the wall and elastic stresses in the UCM fluid, $G/H \sim \eta/\tau_R$, or $\tau_R G/\eta \sim H$. One might expect that instability will cease to exist if the elastic stresses in the wall are much greater than those in the fluid, and this is consistent with the prediction that instability ceases to exist above a critical value of $\bar{W}$. This

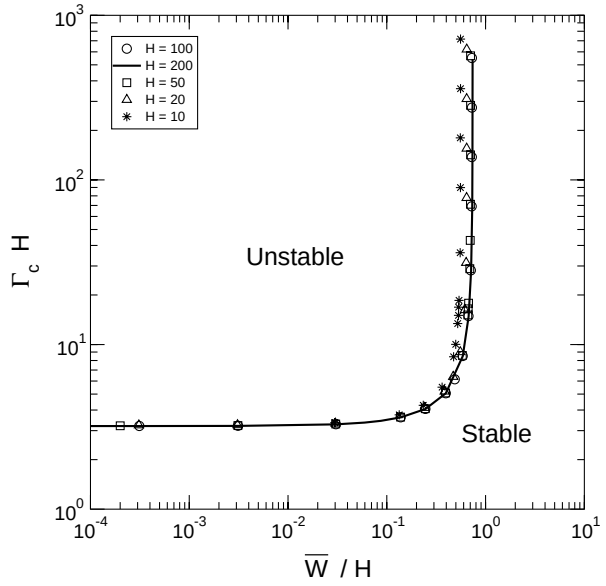

Fig. 13. Data collapse for $H \gg 1$: $\Gamma_c H$ vs. $\bar{W}/H$ for $\eta_r = 0$.

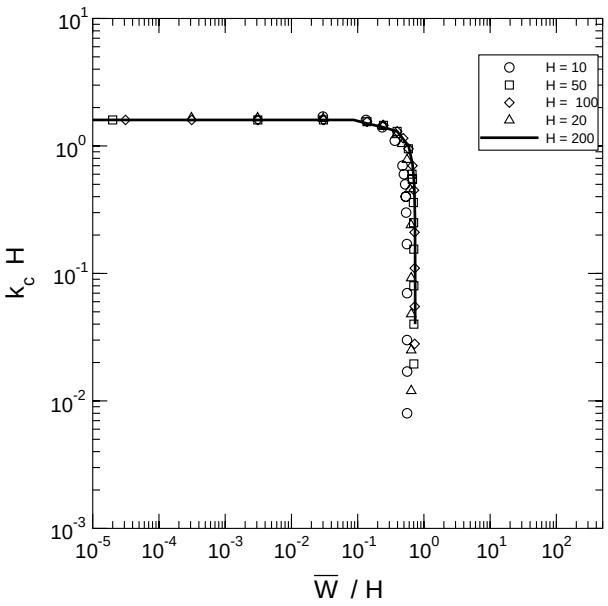

Fig. 14. Data collapse for $H \gg 1$: $k_c H$ vs. $\bar{W}/H$ for $\eta_r = 0$.

prediction can also be interpreted in terms of timescales: instability will not occur unless the fluid can relax its stresses sufficiently quickly relative to the wall relaxation time η/G.

3.4. Comparison with the neo-Hookean solid model

In this section, we compare the results for Γ_c versus $\bar{W}$ (see Fig. 10) obtained using the linear viscoelastic model for the solid with the results obtained using a neo-Hookean model. The linearized governing equations and interface conditions for the stability of a Newtonian fluid past a neo-Hookean solid were presented in the work of Gkanis and Kumar [15], and we have adapted their formulation for the stability of UCM fluid flow past a neo-Hookean solid. The reader is referred to [15] for details of the formualtion. Briefly, the use of the neo-Hookean solid leads to the following modifications in the stability analysis when compared to the linear elastic solid:

- The base state of the neo-Hookean solid has a first normal stress difference, which makes a nontrivial contribution in the linearized *shear stress* condition at the fluid-solid interface. This contribution is akin to what is well known in the stability of the interface between two UCM fluids [16,17]. This jump in the first normal stress difference in the base state between the Newtonian fluid and the neo-Hookean solid gives rise to a high-k instability, which is absent in the case of linear elastic solid model and persists at all $k \gg 1$ when the interfacial tension between the fluid and the solid is zero. The unstable modes for $k \gg 1$ are removed when there is a nonzero interfacial tension between the fluid and the solid. However, for $H > 2$, the critical Γ required to destabilize the high-k modes is *larger* than that required to destabilize the $k \sim \mathrm{O}(1)$ instability which is existent already in the linear elastic solid model.
- The linearized incompressibility equation for a neo-Hookean solid has one additional term due to the nonlinear nature of the incompressibility condition.

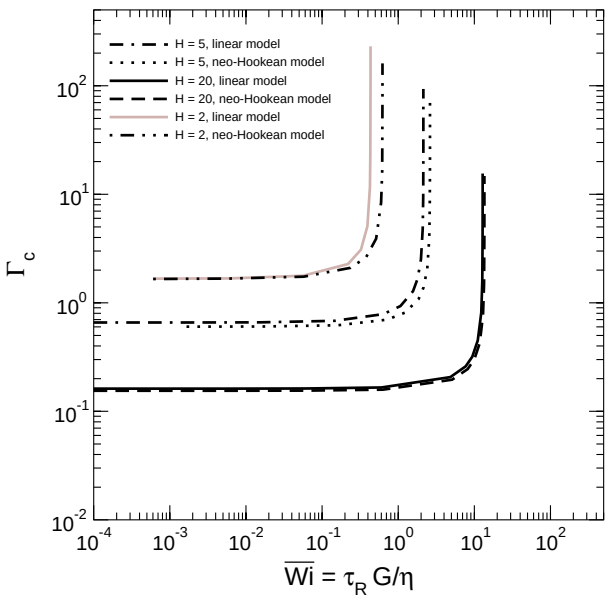

Fig. 15. Comparison of Γ_c vs. $\bar{W}$ for different values of H obtained for a linear viscoelastic solid with $\eta_r = 0$ and a neo-Hookean solid.

- The linearized z-momentum equation for the neo-Hookean solid has one additional term due to the nonlinear coupling between the pressure in the solid and the finger tensor in the expression for the first Piola-Kirchoff stress tensor.
- The tangential stress condition at the interface also has one additional term that arises due to an interaction between the base state deformation gradient in the solid and the vertical gradients in the vertical displacement of the interface.

Fig. 15 shows the variation of Γ_c obtained from the linear viscoelastic solid model (with $\eta_r = 0$) and the neo-Hookean model for the stability of the UCM fluid, for different values of H. The general trend seen is that the neo-Hookean model tends to decrease Γ_c and increase $\bar{W}_{max}$, i.e., it enlarges the zone of instability in the $\Gamma_c - \bar{W}$ plane. The differences between the two solid models diminish as H increases. This comparison shows that the linear elastic solid model gives rise to reasonably accurate predictions even though Γ_c is not strictly small compared to 1. This is true for $H \geq 2$; as H decreases the difference between the models becomes more profound because the higher-k modes of the neo-Hookean model become unstable before the $k \sim O(1)$ modes.

4. Conclusions

The stability of plane Couette flow of an upper-convected Maxwell fluid past a linear viscoelastic solid was analyzed in the creeping-flow limit. It was shown that wall elasticity has a destabilizing effect on one of the two discrete modes of G–L [9] obtained for rigid channels, while finite fluid elasticity has a stabilizing effect on the unstable mode of KFP [2] obtained for Couette flow of a Newtonian fluid past a linear viscoelastic solid. More importantly, we have shown that at finite Γ and W there is only one unstable mode. This mode merges with one of the stable G–L modes as $\Gamma \to 0$ at fixed W, and with the unstable KFP mode as $W \to 0$ at fixed Γ. Thus, we have shown that the continuation of the stable G–L modes to finite wall deformability does not give rise to any *new* unstable modes for the case of plane Couette flow of a UCM fluid past a linear viscoelastic solid. The parameter regime at which this instability exists can be presented in terms of Γ_c versus $\bar{W}$ plots, where $\bar{W} = \tau_R G/\eta$ is a flow-independent modified Weissenberg number. These plots showed that the instability exists in a finite region in the $\Gamma_c - \bar{W}$ plane, when $\Gamma_c > \Gamma_{c,Newt}$ and $\bar{W} < \bar{W}_{max}$, where $\Gamma_{c,Newt}$ is the limiting value of Γ found for Newtonian fluids by KFP [2]. The variation of the maximum value of $\bar{W}$ below which instability occurs showed that $\bar{W}_{max} \propto H$ for $H \gg 1$ regardless of η_r, while the instability ceases to exist for nonzero $\bar{W}$ when H is sufficiently smaller than one and $\eta_r \neq 0$. The variation of Γ_c with $\bar{W}$ for different H was shown to collapse onto a single master curve when plotted in terms of $\Gamma_c H$ and $\bar{W}/H$ in the limit $H \gg 1$. Although the present work was restricted to the UCM model, the instability studied here is expected to carry over to Oldroyd-B fluids as well for reasons explained in Section 3.2.

Finally, it is useful to estimate the typical parameter regime in which the predicted instability could be realized in an experiment. The shear modulus of typical aqueous polymer gels can be estimated to be around 10^4 Pa, while a representative viscosity of polymeric liquids is around 10^2 N s m^{-2}, and the relaxation time τ_R can range from 10^{-2} to 1 s. From these values, the modified $\bar{W}$ can be estimated to be around 1 to 100. From the plot for $\bar{W}_{max}$ versus H (Fig. 12), it can be concluded that the present instability is expected to occur for polymeric liquids flowing past deformable walls of (nondimensional) thickness $H > 10$.

Acknowledgements

SK thanks the Shell Oil Company Foundation for support through its Faculty Career Initiation Funds program, and 3M for a Nontenured Faculty Award. Also, acknowledgment is made to the Donors of the Petroleum Research Fund, administered by the American Chemical Society, for partial support of this research.

References

[1] P. Krindel, A. Silberberg, Flow through gel-walled tubes, J. Colloid Interface Sci. 71 (1979) 34–50.
[2] V. Kumaran, G.H. Fredrickson, P. Pincus, Flow induced instability of the interface between a fluid and a gel at low Reynolds number, J. Phys. II (Fr.). 4 (1994) 893–904.
[3] V. Kumaran, Stability of the viscous flow of a fluid through a flexible tube, J. Fluid. Mech. 294 (1995) 259–281.
[4] V. Kumaran, R. Muralikrishnan, Spontaneous growth of fluctuations in the viscous flow of a fluid past a soft interface, Phys. Rev. Lett. 84 (2000) 3310–3313.
[5] R. Muralikrishnan, V. Kumaran, Experimental study of the instability of viscous flow past a flexible surface, Phys. Fluids. 14 (2002) 775–780.
[6] V. Shankar, V. Kumaran, Stability of non-parabolic flow in a flexible tube, J. Fluid. Mech. 395 (1999) 211–236.
[7] V. Shankar, V. Kumaran, Stability of fluid flow in a flexible tube to non-axisymmetric disturbances, J. Fluid. Mech. 408 (2000) 291–314.
[8] V. Shankar, V. Kumaran, Stability of wall modes in fluid flow past a flexible surface, Phys. Fluids. 14 (2002) 2324–2338.
[9] V.A. Gorodtsov, A.I. Leonov, On a linear instability of plane parallel Couette flow of viscoelastic fluid, J. Appl. Math. Mech. 31 (1967) 310–319.
[10] H.J. Wilson, M. Renardy, Y. Renardy, Structure of the spectrum in zero Reynolds number shear flow of the UCM and Oldroyd-B liquids, J. Non-Newtonian Fluid Mech. 80 (1999) 251–268.
[11] M.D. Graham, Effect of axial flow on viscoelastic Taylor–Couette instability, J. Fluid. Mech. 360 (1998) 341–374.
[12] M. Renardy, Y. Renardy, Linear stability of plane Couette flow of an upper convected Maxwell fluid, J. Non-Newtonian Fluid Mech. 22 (1986) 23–33.
[13] M. Renardy, A rigorous stability proof for plane Couette flow of an upper convected Maxwell fluid at zero Reynolds number, Euro. J. Mech. B: Fluids 11 (1992) 511–516.
[14] R. Sureshkumar, A.N. Beris, Linear stability analysis of viscoelastic Poiseuille flow using an Arnoldi based orthogonalization algorithm, J. Non-Newtonian Fluid. Mech. 56 (1995) 151–182.
[15] V. Gkanis, S. Kumar, Instability of creeping Couette flow past a neo-Hookean solid, Phys. Fluids 15 (2003) 2864–2871.
[16] Y. Renardy, Stability of the interface in two-layer Couette flow of upper convected Maxwell liquids, J. Non-Newtonian Fluid Mech. 28 (1988) 99–115.
[17] K. Chen, Elastic instability of the interface in Couette flow of two viscoelastic liquids, J. Non-Newtonian Fluid Mech. 40 (1991) 261–267.
[18] R.G. Larson, Constitutive Equations for Polymer Melts and Solutions, Butterworths, Boston, 1988.
[19] R. Sureshkumar, M.D. Smith, R.C. Armstrong, R.A. Brown, Linear stability and dynamics of viscoelastic flows using time dependent simulations, J. Non-Newtonian Fluid. Mech. 82 (1999) 57–104.